Copepod flow modes and modulation: a modelling study of the water currents produced by an unsteadily swimming copepod

Houshuo Jiang[1],* and J. Rudi Strickler[2]

[1]*Department of Applied Ocean Physics and Engineering, Woods Hole Oceanographic Institution, Woods Hole, MA 02543, USA*
[2]*Great Lakes WATER Institute, University of Wisconsin-Milwaukee, Milwaukee, WI 53204, USA*

Video observation has shown that feeding-current-producing calanoid copepods modulate their feeding currents by displaying a sequence of different swimming behaviours during a time period of up to tens of seconds. In order to understand the feeding-current modulation process, we numerically modelled the steady feeding currents for different modes of observed copepod motion behaviours (i.e. free sinking, partial sinking, hovering, vertical swimming upward and horizontal swimming backward or forward). Based on observational data, we also reproduced numerically a modulated feeding current associated with an unsteadily swimming copepod. We found that: (i) by changing its propulsive force, a copepod can switch between different swimming behaviours, leading to completely different flow-field patterns in self-generated surrounding flow; (ii) by exerting a time-varying propulsive force, a copepod can modulate temporally the basic flow modes to create an unsteady feeding current which manipulates precisely the trajectories of entrained food particles over a long time period; (iii) the modulation process may be energetically more efficient than exerting a constant propulsive force onto water to create a constant feeding current of a wider entrainment range. A probable reason is that the modulated unsteady flow entrains those water parcels containing food particles and leaves behind those without valuable food in them.

Keywords: calanoid copepod; swimming behaviour; flow-field pattern; unsteady; modulation; hydrodynamics

1. INTRODUCTION

Numerous observations have shown that calanoid copepods display a variety of free-swimming behaviours (for a partial literature list on free-swimming behaviours of various copepod species observed with microcinematography and video microscopy, see Jiang *et al.* 2002a). Several studies have also measured the flow fields created by free-swimming copepods at one or several instants of time by tracking algal particles surrounding the copepods over a short time interval (Strickler 1982; Tiselius & Jonsson 1990; Yen *et al.* 1991; Bundy & Paffenhöfer 1996). The swimming behaviours studied include hovering, horizontal swimming (backward or forward), upward swimming and free sinking. In addition, these studies show that the flow-field properties, such as flow geometry, flow rates, flow velocities and velocity gradients, vary for different free-swimming behaviours. Such a dependence of flow-field properties on free-swimming behaviours has been confirmed by a hydrodynamic modelling study using a Stokes flow model for the flow fields generated by a negatively buoyant self-propelled body (Jiang *et al.* 2002a) and a companion numerical simulation study using computational fluid dynamics (CFD; Jiang *et al.* 2002b).

Recently, Malkiel *et al.* (2003) developed a method of using digital holographic cinematography to measure the three-dimensional instantaneous velocity field around a free-swimming copepod. For a species of coastal and freshwater copepod, *Diaptomus minutus*, they observed a three-dimensional velocity field with a circulatory flow pattern as viewed in the frame of reference fixed on the copepod's body. In this case, the copepod exhibits an interesting behaviour, i.e. the copepod sinks slowly while still beating its cephalic appendages. The beating movement of the cephalic appendages produces a propulsive force against the excess weight of the copepod, making the copepod sink at a rate that is lower than its terminal sinking speed. (We term this behaviour 'partial sinking' hereafter.) An earlier observation by Bundy & Vanderploeg (2002) also reported that a calanoid copepod species, *Skistodiaptomus oregonensis*, uses a suspension-feeding mode while sinking (i.e. it sinks slowly while still beating its cephalic appendages).

In this paper, we will first apply the hydrodynamic model developed by Jiang *et al.* (2002a) to the partial sinking behaviour. Then, based on a full range of parametric studies, we show an integrative picture of

how flow-field patterns vary systematically and continuously with different basic steady translational swimming behaviours, i.e. free sinking, partial sinking, hovering, vertical swimming upward and horizontal swimming backward or forward. The flow fields created with respect to these basic steady translational swimming behaviours are then taken as the basic flow modes.

To study these basic flow modes, we do not mean that the water currents created by copepods should be viewed as constant or steady. On the contrary, these basic flow modes can be regarded as the 'building blocks' to construct more complex unsteady flows. Within the time-space of 10 s, a copepod frequently switches between swimming behaviours and changes its swimming speed even for the same kinds of swimming behaviours. All these may lead to unsteadiness in the flow field around the copepod (i.e. unsteadiness at copepod body scale). Owing to the high-frequency (20–80 Hz) beating motion of copepod cephalic appendages at the appendage scale (20–200 µm), near the appendages and over a time-scale of milliseconds, the flow is always unsteady. However, such unsteadiness at very fine temporal and spatial scales cannot penetrate beyond the viscous length scale (less than 150 µm; Jiang *et al.* 2002a) and therefore is not considered in this study. What concerns us is the flow unsteadiness at the copepod body scale and over a time-scale of a few seconds.

Although unsteadiness is common, no previous observations have provided measurements of the (unsteady) flow field as a time-series (a series of snapshots) over a long time period (e.g. tens of seconds). However, such a time-series is key to the understanding of the correlations among a copepod's ever-changing swimming behaviour, unsteady flows around its body and trajectories of entrained algal particles over long intervals. In this study, we will reconstruct an unsteady flow field around a free-swimming copepod observed over a long time period. To achieve this, we will employ a method of modulating the basic flow modes based on an observed time history of the copepod's swimming velocity. We will test a hypothesis which suggests that by adjusting the propulsive force to achieve certain sequences of swimming behaviours (i.e. by modulating some basic flow modes that a copepod is allowed to have), a copepod can control the unsteady water currents it creates around its body, and therefore, can manipulate precisely the trajectories of algal particles entrained in the currents over long intervals. Another interesting question we want to answer is how the mechanical energetic efficiency for scanning a volume of water varies during this modulation process. For answering this question, CFD simulations of flow field around a model copepod will be performed. From CFD simulation data, we will calculate the scanned volume of water (in terms of volumetric flux passing through the copepod's capture area), mechanical power input for creating the flow field around the copepod and the scanning efficiency (in terms of the ratio between volumetric flux and mechanical power input) for various sinking speeds within the partial sinking behaviour.

2. MATERIAL AND METHODS

We thank Dr J. Yen for allowing us to use a portion of videotaped observation made by her in JRS' laboratory on free-swimming adult females of *Euchaeta rimana* (prosome length of approx. 2.5 mm). The details of the observation can be found in Yen *et al.* (1991), in which the steady feeding currents created by a perfectly hovering *E. rimana* have been well examined. The portion of observation that we have analysed for the present work is relatively longer in time duration (approx. 21.67 s) and has not been analysed or published before. Although the observation was two-dimensional, the copepod remained in focus during the whole unsteady swimming event. An algal particle that the copepod was interacting with was also in the plane of focus during the whole event. The portion of the videotape was first digitized into video images at 640×480 pixels with 8 bits of pixel depth by using image-grabbing software (ADOBE PREMIERE PRO v. 1.5). In total, 650 consecutive frames were obtained at a rate of 30 frames per second. Frame-by-frame analysis was then made with ADOBE ILLUSTRATOR v. 8.0 by reading pixel numbers manually. To determine the time history of the copepod's unsteady swimming velocity, a time-series of positions of the copepod's rostrum was obtained with respect to the position of a non-moving particle far away from the copepod. To determine the trajectory of the previously mentioned algal particle that the copepod was interacting with, a time-series of positions of the algal particle was also obtained. The trajectory of the algal particle was plotted corresponding to a frame of reference fixed on the copepod.

A large part of this paper is devoted to hydrodynamic modelling and CFD simulations for carrying out a full range of parametric studies on the basic flow modes corresponding to the basic steady translational swimming behaviours of copepods, and for reconstructing the unsteady flow field created by the observed *E. rimana* female in unsteady swimming. The purpose is to provide a mechanistic understanding of the interplay between a copepod's ever-changing swimming behaviour, unsteady flows around its body, and trajectories of entrained algal particles over long intervals. We feel it is more appropriate not to separate the modelling/simulation methods from the modelling/simulation results. Therefore, we choose not to present the methods in this section. The methods are to be presented along with the results in §2b.

(a) *Observational results*

Figure 1 illustrates the observed unsteady swimming behaviour of an *E. rimana* female and also shows a trajectory of an entrained algal particle over a long interval (approx. 21.67 s). The time history of the copepod's translational swimming velocity components are shown in figure 2. The screen horizontal rightward direction is the positive x-direction and the screen vertical upward direction is the positive z-direction.

The observed behaviour can be divided into two phases; at the very beginning of phase 1 (figure 1a), the copepod swam horizontally slowly in a positive x-direction (figure 2a) with the left branch of its first antennae pointing towards the entrained algal particle. The copepod's posterior–anterior body axis was aligned with the z-direction, with its anterior pointing upward. Then, the copepod rotated slowly around its posterior–anterior body axis until its ventral body part faced the entrained algal particle. Simultaneously, the copepod started to sink at an accelerated speed (figure 2b). Phase 1 lasted 4.33 s (frame 0–130).
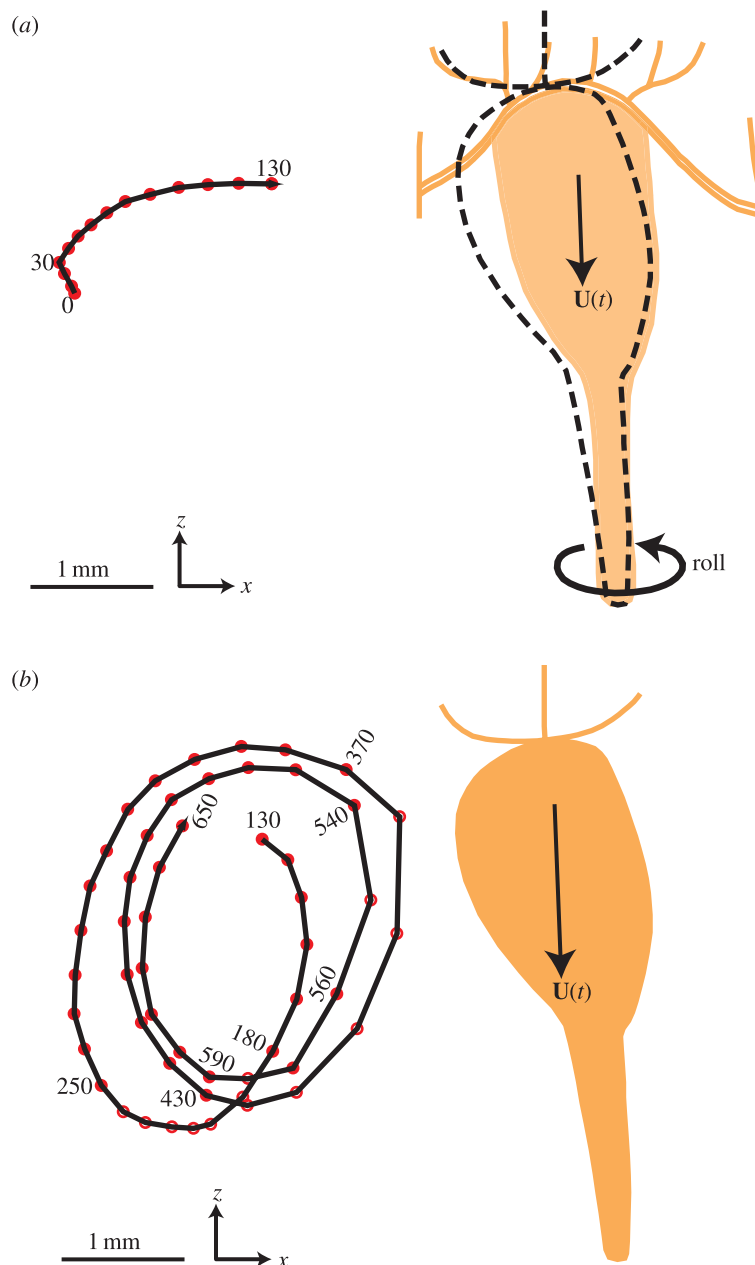
Figure 1. An observed free-swimming behaviour of an *Euchaeta rimana* female. The results were obtained through frame-by-frame analysis of a video clip of 650 frames in total at 30 frames per second so that the time duration was approximately 21.67 s. A trajectory of an entrained algal particle is also shown with respect to a frame of reference fixed on the copepod's body (data points were shown every 10 frames). (*a*) Frame 0–130, the copepod sank obliquely at a time-varying velocity and simultaneously rotated around its anterior–posterior body axis. The rotation started from the body position in orange and ended at the body position in dashed lines. (*b*) Frame 130–650, the copepod sank obliquely at a time-varying velocity without body rotation. Note that the algal trajectory was a spiral-like unclosed curve.

During phase 2 (figure 1*b*), the copepod maintained a constant body posture with its anterior pointing upward and ventral body part facing left towards the entrained algal particle. The copepod sank obliquely with time-varying velocity components in both the vertical and horizontal directions (figure 2). Phase 2 lasted 17.34 s (frame 130–650). The total travelling distance of the copepod was approximately 38.8 mm in the negative z-direction and 3.2 mm in the positive x-direction. During the whole event (phase 1 and phase 2), the trajectory of the entrained algal particle was always under the influence of the unsteady flow field created by the copepod at its body scale. As seen from the point of view of the copepod, the entrained algal particle travelled along a spiral-like unclosed trajectory (figure 1*b*).

(b) *Hydrodynamic modelling and simulation studies*
(i) *Basic flow modes of copepod-created flows*
We define the basic flow modes as the flow fields created by copepods in basic steady translational swimming behaviours, i.e. free sinking, hovering, vertical swimming upward, horizontal swimming backward or forward and partial sinking. The steady flow fields associated with the first five among the six behaviours have been examined previously by using a Stokes flow model for flow field created by a negatively buoyant self-propelled body (Jiang *et al.* 2002*a*). The same Stokes flow model is used here to examine the flow field corresponding to the steady partial sinking behaviour. The details of the Stokes flow model have been presented in Jiang *et al.* (2002*a*). Here, we recapitulate the main results: when the model spherical copepod swims steadily along a vertical
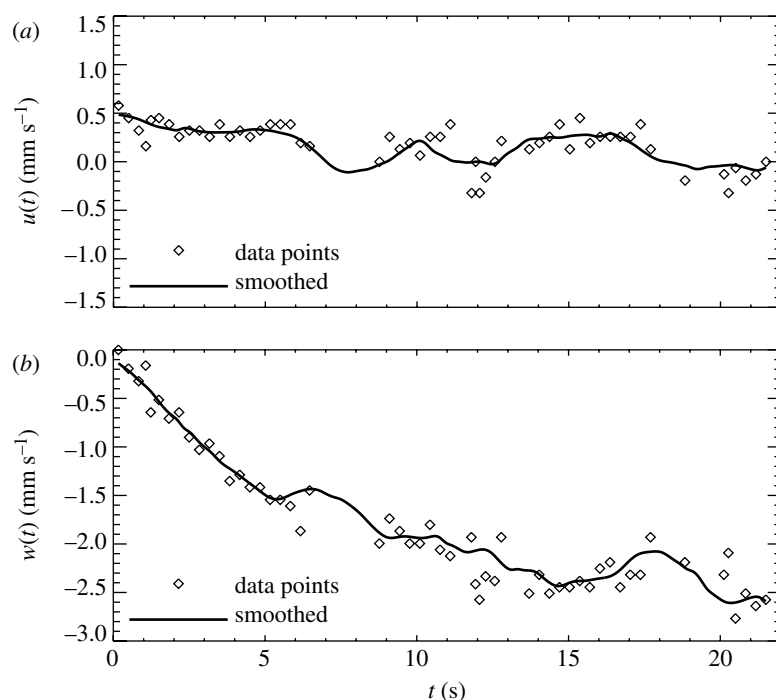
Figure 2. Time history of the swimming velocity for the swimming event shown in figure 1. (*a*) Horizontal swimming velocity, *u*, versus time, *t*. (*b*) Vertical sinking velocity, *w*, versus time, *t*.

plane at a swimming velocity $\mathbf{U}=u\mathbf{i}+w\mathbf{k}$, where u is the horizontal component of the velocity vector with $\mathbf{i}$ denoting the unit vector in the horizontal x-direction and w is the vertical component of the velocity vector with $\mathbf{k}$ denoting the unit vector in the vertical z-direction, the propulsive force, $\mathbf{f}$, that the model copepod exerts on the water can be found as

$$\mathbf{f} = \frac{-6\pi\mu a u}{1-\frac{1}{2}\left(\frac{3}{\beta}-\frac{1}{\beta^3}\right)}\mathbf{i} + \frac{\left(-6\pi\mu a w - W_{\text{excess}}\right)}{1-\frac{1}{4}\left(\frac{3}{\beta}+\frac{1}{\beta^3}\right)}\mathbf{k}, \qquad (2.1)$$

where μ is the dynamic viscosity ($1.390\times10^{-3}\,\text{kg m}^{-1}\,\text{s}^{-1}$ for seawater of salinity $S=35$ at $10°\text{C}$ and at one normal atmosphere), a is the radius of the model copepod, W_{excess} (greater than 0) is the magnitude of the model copepod's excess weight and β is a parameter determined by the application point of the propulsive force relative to the centre of the model copepod. All these model parameters are the same as those used in Jiang *et al.* (2002*a*). For the steady partial sinking behaviour (figure 3*a*), the swimming velocity vector reduces to $\mathbf{U}=w\mathbf{k}$, with $u=0$ and $w<0$; w is a given constant for steady partial sinking, the magnitude of which is less than the copepod's terminal sinking speed. Correspondingly, the propulsive force, $\mathbf{f}$, reduces to

$$\mathbf{f} = \frac{\left(-6\pi\mu a w - W_{\text{excess}}\right)}{1-\frac{1}{4}\left(\frac{3}{\beta}+\frac{1}{\beta^3}\right)}\mathbf{k}. \qquad (2.2)$$

Thus, for a given partial sinking velocity w, the propulsive force is calculated according to equation (2.2), and then the flow velocity vector field around the model copepod can be calculated (see Jiang *et al.* 2002*a* for details). For partial sinking behaviour, the free body diagrams (FBDs) of the model copepod and the surrounding water are drawn in figure 3*b*,*c*, respectively. From the model copepod's point of view, the thrust, $\mathbf{f}'$, obtained by the model copepod from the water surrounding its cephalic appendages, is applied along the same direction as the drag force, $\mathbf{F}$, exerted by the surrounding water on the model copepod's main body (figure 3*b*). The force balance is that the upward thrust, $\mathbf{f}'$, plus the upward drag force, $\mathbf{F}$, counterbalances the downward

excess weight. From the surrounding water's point of view, the propulsive force, $\mathbf{f}$, that the model copepod exerts on the water surrounding its cephalic appendages, is applied along the same direction as the drag force, $\mathbf{F}'$, acting on the surrounding water by the model copepod's main body (figure 3*c*). By contrast, for other steady translational swimming behaviours, such as hovering, vertical swimming upward and horizontal swimming backward or forward, $\mathbf{f}'$ and $\mathbf{F}$ (or, $\mathbf{f}$ and $\mathbf{F}'$) are applied in opposite directions. For copepods displaying the partial sinking behaviour, this unique property in force configuration leads to the unique circulatory flow pattern as observed by Malkiel *et al.* (2003). Since the copepod pumps a volume of water in the direction against the flow associated with its sinking motion, a circulatory flow pattern is formed as viewed in a frame of reference fixed on the copepod's body. This is the principal mechanism in creating the observed circulatory flow pattern.

To show an integrative picture, the modelled flow patterns for the steady partial sinking behaviour are presented along with those for other basic steady translational swimming behaviours. The basic steady translational swimming behaviours along the vertical direction (z-direction) can be uniformly described by one parameter, namely $w/|\mathbf{w}_{\text{terminal}}|$ (with the horizontal swimming velocity $u=0$), where w is the vertical swimming velocity and $\mathbf{w}_{\text{terminal}}$ is the terminal sinking velocity. $w/|\mathbf{w}_{\text{terminal}}|=-1$ for free sinking, $-1<w/|\mathbf{w}_{\text{terminal}}|<0$ for partial sinking, $w/|\mathbf{w}_{\text{terminal}}|=0$ for hovering, and $w/|\mathbf{w}_{\text{terminal}}|>0$ for upward swimming. (Note that all calculations are in three-dimensional though the results have to be often plotted on a two-dimensional plane.) Figure 4 shows the flow velocity fields associated with these vertical swimming behaviours. Figure 5 shows three-dimensional algal trajectories passing through the model copepod's capture area for each of these vertical swimming behaviours. Both figures use a frame of reference fixed on the model copepod. Generally, each flow pattern consists of three-dimensional flow geometry (figure 5), and there exist a dorsal–ventral asymmetry (side views shown in figure 4) and a left–right symmetry (front views not shown) in each flow field. For free
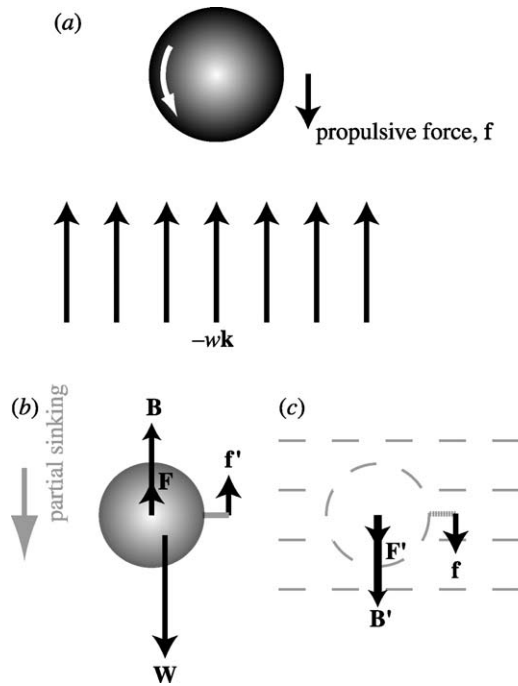
Figure 3. (*a*) Schematic of the hydrodynamic model of a negatively buoyant copepod performing partial sinking (i.e. by definition, the sinking speed is less than the copepod's terminal sinking speed). The model copepod consists of a spherical body and a point force, **f**, located outside the spherical body. The frame of reference is fixed on the body, so that the steady partial sinking motion of the copepod is transformed into a constant flow coming from below the copepod. The curved arrow indicates the torque acting on the model copepod due to the reaction force of **f**. Note that for simplicity the balance of the torques on the model copepod is not considered here. We assume that choosing a suitable centre of mass relative to the centre of volume enforces the torque balance. (*b*) The FBD for the model copepod performing partial sinking. **W** stands for the copepod's weight acting at the centre of mass; **B** stands for buoyancy acting at the centre of volume of the copepod; **F** stands for the drag force of the surrounding water flow over the surface of the body; **f**′ is the reaction force of the water acting on the copepod's cephalic appendages. (*c*) FBD of the surrounding water. **f** is the point force exerted on the water by the copepod, representing the effect of the beating movement of the cephalic appendages; **F**′ + **B**′ stands for the force of the copepod on the surrounding water through the body–fluid interface. Note that **f**′ = −**f**, **F**′ = −**F**, and **B**′ = −**B** (Newton's third law).

sinking ($w/|\mathbf{w}_{\text{terminal}}| = -1$), the flow comes from below the copepod and no circulatory flow pattern is formed (or we can say the size of the eddy becomes infinitesimal). For partial sinking ($-1 < w/|\mathbf{w}_{\text{terminal}}| < 0$), a circulatory flow pattern of finite eddy size is formed; with increasing $w/|\mathbf{w}_{\text{terminal}}|$ from -1 to 0, the size of the eddy increases (figure 4 and the same box-size views for partial sinking in figure 5). Trajectories of particles passing through the copepod's capture area are closed three-dimensional curves at the ventral side of the body (partial sinking in figure 5). For hovering ($w/|\mathbf{w}_{\text{terminal}}| = 0$), it can be imaged that the circulatory eddy becomes infinite (i.e. particles travel from $+\infty$ to $-\infty$). For upward swimming ($w/|\mathbf{w}_{\text{terminal}}| > 0$), no circulatory flow pattern is formed; with increasing $w/|\mathbf{w}_{\text{terminal}}|$, the flow pattern changes from a feeding current of more cone-shaped geometry to a swimming current of more cylindrical geometry (i.e. force monopole versus force dipole; see Jiang *et al.* 2002*a* for explanation).
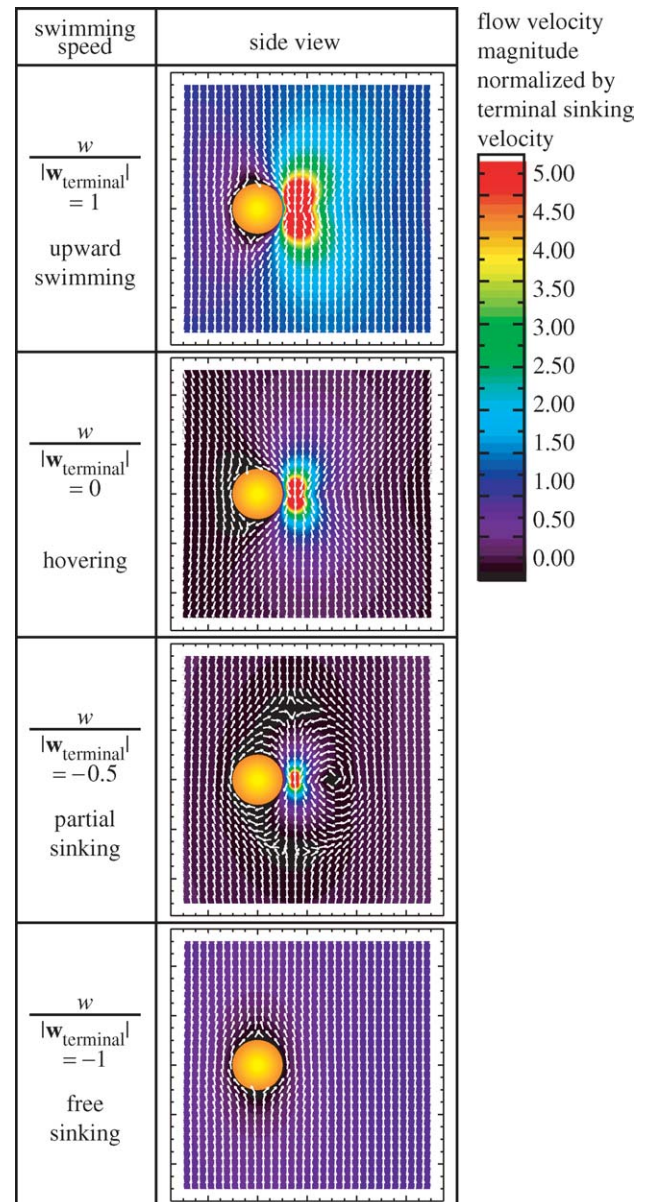
Figure 4. Basic flow modes created by the model copepod performing several basic steady translational swimming behaviours along the vertical direction, i.e. free sinking ($w/|\mathbf{w}_{\text{terminal}}| = -1$), partial sinking ($-1 < w/|\mathbf{w}_{\text{terminal}}| < 0$), hovering ($w/|\mathbf{w}_{\text{terminal}}| = 0$) and upward swimming ($w/|\mathbf{w}_{\text{terminal}}| > 0$). Here, w is the vertical (z-direction) swimming velocity component, and $\mathbf{w}_{\text{terminal}}$ is the model copepod's terminal sinking velocity. By convention, the positive z-direction is opposite to the direction of gravity. The uniform length vectors show the flow direction and the colour contours of flow velocity magnitudes (normalized by copepod terminal sinking velocity) show the flow intensity. A frame of reference fixed on the copepod's body is used. The vector and contour plots are drawn along the median plane ($y = 0$) of the model copepod.

The calculations also enable us to determine the size of the circulatory eddy and the looping time of several representative particle trajectories (table 1). It is clear from these data that $w/|\mathbf{w}_{\text{terminal}}|$ is in the range -0.50 to -0.25 corresponding to the characteristic looping time of approximately 9.0 s as observed by Malkiel *et al.* (2003). In addition, the flow velocity vector plots show two stagnation points, one above and another below the model copepod, for the steady partial sinking behaviour (figure 4). This is also consistent with the observation by Malkiel *et al.* (2003).
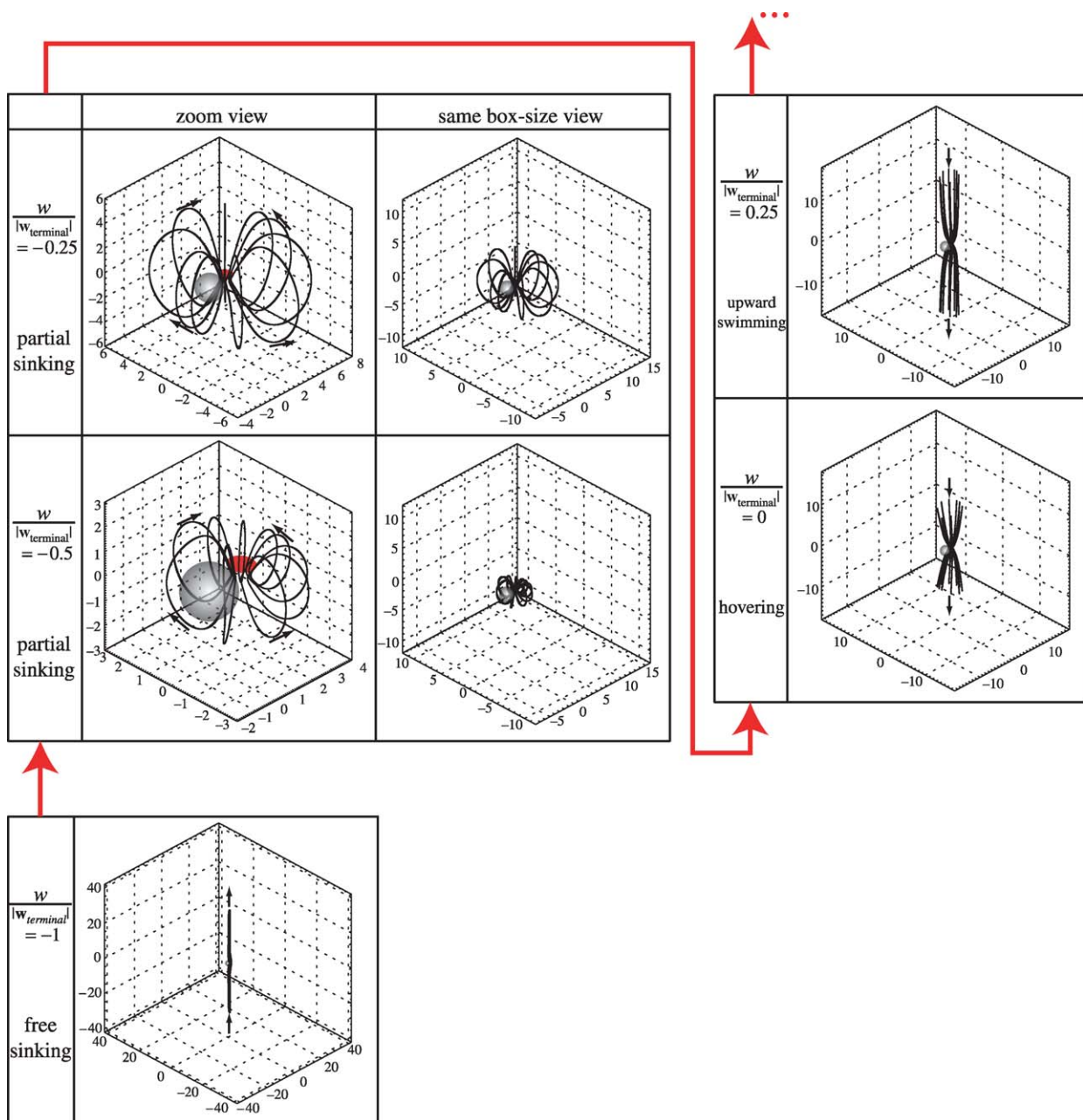
Figure 5. Three-dimensional algal trajectories passing through the model copepod's capture area for basic steady translational swimming behaviours along the vertical direction. The red arrows indicate the direction along which $w/|\mathbf{w}_{terminal}|$ increases from -1 to 0.25, i.e. the vertical swimming behaviour evolves: free sinking→partial sinking→hovering→upward swimming. See figure 4 caption for further explanation.

Table 1. Steady partial sinking behaviour. (Eddy sizes of the circulatory flow patterns and looping times of 11 representative particles passing through the capture area of the model copepod for several $w|\mathbf{w}_{terminal}|$ ratios.)

	$w/|\mathbf{w}_{terminal}| = -0.75$	$w/|\mathbf{w}_{terminal}| = -0.50$	$w/|\mathbf{w}_{terminal}| = -0.25$	$w/|\mathbf{w}_{terminal}| = -0.125$
eddy size	≈0.5 body length	≈1 body lengths	≈3 body lengths	≈6 body lengths
looping times (s) of 11 representative particles	0.84, 0.85, 0.87, 0.90, 0.96, 1.07, 1.29, 1.76, 2.98, 0.97, 1.58	2.57, 2.60, 2.66, 2.77, 2.93, 3.18, 3.59, 4.35, 6.25, 3.21, 4.93	15.18, 15.27, 15.46, 15.71, 15.94, 15.99, 15.63, 14.90, 14.37, 18.75, 22.01	80.53, 80.49, 80.22, 79.30, 77.12, 73.16, 67.60, 61.86, 58.14, 97.67, 88.27

The basic steady translational swimming behaviours along the horizontal direction (x-direction) can also be uniformly described by another parameter, namely $u/|\mathbf{w}_{terminal}|$ (with the vertical swimming velocity $w=0$), where u is the horizontal swimming velocity. $u/|\mathbf{w}_{terminal}|<0$ for backward swimming and $u/|\mathbf{w}_{terminal}|>0$ for forward swimming.

Figure 6 shows the respective three-dimensional algal trajectories passing through the model copepod's capture area. For horizontal swimming, no circulatory flow pattern is formed; with increasing the absolute value of $u/|\mathbf{w}_{terminal}|$, the flow pattern changes from a feeding current of more cone-shaped geometry to a swimming current of more cylindrical
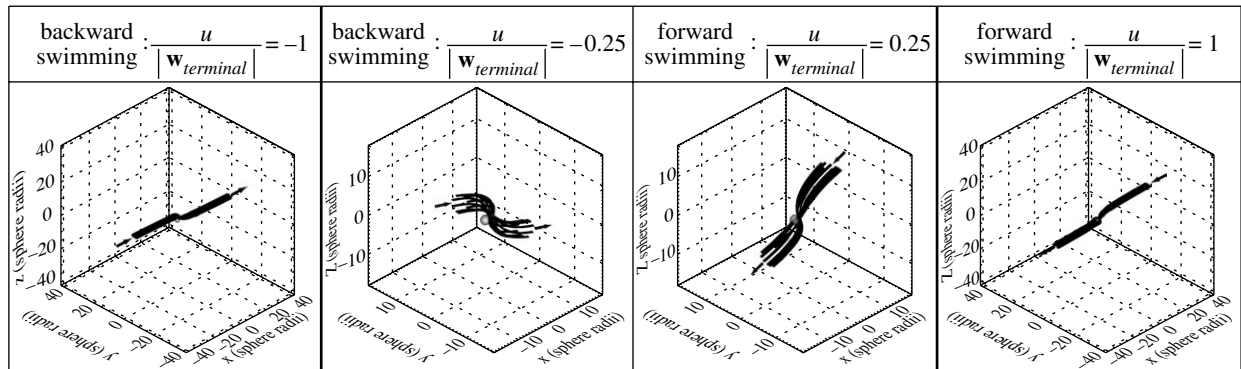
Figure 6. Three-dimensional algal trajectories passing through the model copepod's capture area for basic steady translational swimming behaviours along the horizontal direction, i.e. horizontal swimming backward ($u/|\mathbf{w}_{\text{terminal}}| < 0$) and forward ($u/|\mathbf{w}_{\text{terminal}}| > 0$). Here, u is the horizontal (x-direction) swimming velocity component and $\mathbf{w}_{\text{terminal}}$ is the model copepod's terminal sinking velocity. The positive x-direction is defined as the direction from dorsal to ventral. A frame of reference fixed on the copepod's body is used.

geometry. The flow geometry for horizontal swimming is more horizontally oriented as compared to the vertically oriented flow geometry for hovering/upward swimming.

The vertical, f_z, and horizontal, f_x, components of the propulsive force, $\mathbf{f}$, that the model copepod exerts on the water surrounding its cephalic appendages are plotted as functions of the basic steady translational swimming behaviours (figure 7). The volumetric flux, Q (in units of $\text{m}^3\,\text{s}^{-1}$), passing through the model copepod's capture area is also plotted as functions of the swimming behaviours (figure 8). (Note that $1\,\text{m}^3\,\text{s}^{-1} = 8.64 \times 10^{10}\,\text{ml}\,\text{d}^{-1}$ and that $\text{ml}\,\text{d}^{-1}$ is used by biological oceanographers in the context of the clearance rate.) Based on these results, it is concluded that by exerting different propulsive forces, a copepod can achieve different basic steady translational swimming behaviours, and a copepod's encounter volume varies with different swimming behaviours. Furthermore, our results imply that the influence range as well as the influence direction of the flow field varies for different swimming behaviours. The results of our modelling study confirm the results obtained from the excellent observational and comparative study by Tiselius & Jonsson (1990) who have shown that flow rates (equivalent to volumetric flux) vary significantly for different copepod species with different foraging modes. Owing to the modelling nature of the present study, swimming behaviour has been taken as the only varying parameter. Our parametric modelling study shows that variations in the volumetric flux can be realized solely due to differences in swimming behaviours.

(ii) *Modulation of the basic flow modes*

We propose a new concept for copepod-created flows, namely modulation of the basic flow modes. This is equivalent to a modulation of the propulsive force. As a result, an unsteady flow may be created. As a proof of concept, we reproduce the unsteady flow field for phase 2 of the observed unsteady swimming event of an *E. rimana* adult female (figure 1b) by modulating the propulsive force based on the observed time history of the copepod's swimming velocity (figure 2).

Consider a spherical model copepod of radius, b (figure 9). It applies a time-varying propulsive force, $\mathbf{f}(t)$, at a ventrally located given point, $\mathbf{x}_0$. As a result, the model copepod translates at a time-varying velocity, $\mathbf{U}(t)$. Assume $\mathbf{U}(t)$ is aligned with the median plane (i.e. the x–z plane) of the model copepod and consists of a horizontal component, $u(t)$, and a vertical component, $w(t)$. $u(t)$ and $w(t)$ are exactly the same as those shown in figure 2 (smoothed, frame 130–650). If we totally ignore the inertial effects in the Navier–Stokes equations governing the flow around the spherical model
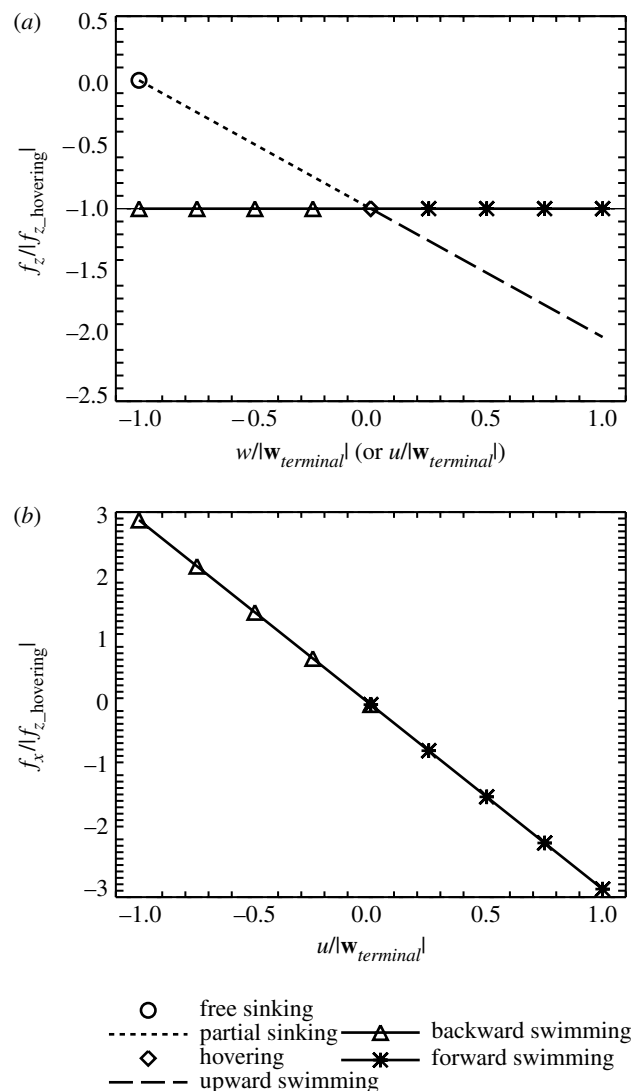

Figure 7. Propulsive force as a function of the basic steady translational swimming behaviours and velocities: (a) for the vertical (z-direction) propulsive force component (f_z); (b) for the horizontal (x-direction) propulsive force component (f_x). All the forces are normalized by the magnitude of the propulsive force calculated for the hovering behaviour ($|f_{z\_\text{hovering}}|$). Note that $f_x = 0$ for free sinking, partial sinking, hovering and upward swimming in this modelling study.

copepod, use a frame of reference fixed on the spherical model copepod, and choose the centre of the sphere as the
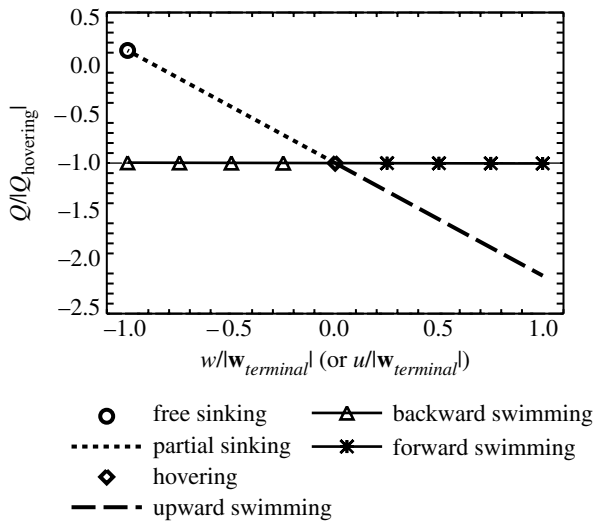
Figure 8. Volumetric flux, Q, through the capture area of the model copepod as a function of the basic steady translational swimming behaviours and velocities. The capture area is defined as an area enclosed by a small horizontal circle ventral to the model copepod (see Jiang *et al.* 2002*a* for details). All the fluxes are normalized by the magnitude of the flux calculated for the hovering behaviour ($|Q_{hovering}|$). Note that fluxes of a negative sign ($-$) are downward (negative z-direction) fluxes.

origin of the frame of reference, we can write down the solution for the time-dependent three-dimensional velocity vector field as

$$u_i(\mathbf{x}, t) = -U_i(t) + \frac{1}{4}\frac{b}{r'}\left(3 + \frac{b^2}{r'^2}\right)U_i(t)$$
$$+ \frac{3}{4}\frac{b}{r'}\left(1 - \frac{b^2}{r'^2}\right)\frac{x_i x_j}{r'^2}U_j(t) + \frac{1}{8\pi\mu}G_{ij}^{SPH}(\mathbf{x}, \mathbf{x}_0)f_j(t),$$
$$(2.3)$$

where the summation convention applies with the indices i, $j = 1, 2, 3$; $r' = |\mathbf{x}|$, and $\mathbf{G}^{SPH}$ is the Green's function for an infinite flow bounded internally by a solid sphere (see Jiang *et al.* 2002*a* for explanation). The unsteady swimming velocity is

$$\begin{pmatrix} U_1(t) \\ U_2(t) \\ U_3(t) \end{pmatrix} \equiv \mathbf{U}(t) = \begin{pmatrix} u(t) \\ 0 \\ w(t) \end{pmatrix},$$
$$(2.4)$$

and the propulsive force is calculated according to

$$\begin{pmatrix} f_1(t) \\ f_2(t) \\ f_3(t) \end{pmatrix} \equiv \mathbf{f}(t) = \begin{pmatrix} f_x(t) \\ 0 \\ f_z(t) \end{pmatrix},$$
$$(2.5)$$

with

$$f_x(t) = \frac{-6\pi\mu b u(t) - (m + m_a)\frac{du(t)}{dt}}{1 - \frac{1}{2}\left(\frac{3}{\beta} - \frac{1}{\beta^3}\right)}$$
$$(2.6)$$

and

$$f_z(t) = \frac{-6\pi\mu b w(t) - W_{excess} - (m + m_a)\frac{dw(t)}{dt}}{1 - \frac{1}{4}\left(\frac{3}{\beta} + \frac{1}{\beta^3}\right)}.$$
$$(2.7)$$

In fact, the propulsive force is calculated from the dynamic equation of the spherical model copepod body including the contribution from body inertia and the added mass term (Jiang 2004). The radius, b, of the spherical model copepod is determined by conserving the body volume of a typical
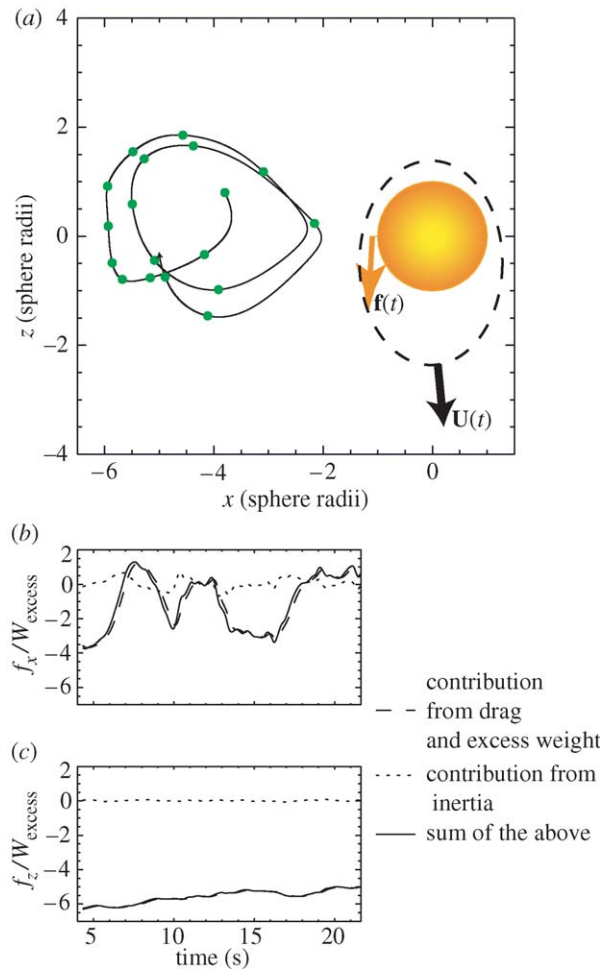
Figure 9. (*a*) Hydrodynamic model for the observed free-swimming behaviour of an *E. rimana* female as shown in figure 1*b*. Also shown is a modelled particle trajectory which resembles the observed algal trajectory of the spiral-like unclosed curve (figure 1*b*). For every 1 s, an instantaneous algal position is shown. A frame of reference fixed on the model copepod's body is used. The model copepod consists of a spherical body with a time-varying propulsive force, $\mathbf{f}(t)$, located ventrally to the model copepod. The whole system swims at a time-varying velocity, $\mathbf{U}(t)$, of the same two components as those shown in figure 2 (4.33–21.67 s). (*b*) The horizontal (x-direction) component, f_x, of the time-varying propulsive force $\mathbf{f}(t)$; (*c*) the vertical (z-direction) component, f_z, of the time-varying propulsive force $\mathbf{f}(t)$. The two force components are normalized by the excess weight (W_{excess}) of the copepod.

E. rimana female. The body volume is calculated approximately as $\pi R^2 L$, where $R = 0.625$ mm is the half body width and $L = 2.5$ mm is the prosome length of the body. The body mass, m, of the spherical model copepod is $4/3\pi b^3 \rho_c$, where ρ_c is the mass density of the copepod. The added mass, m_a, of the spherical model copepod is $2/3\pi b^3 \rho_w$, where ρ_w is the mass density of seawater (1026.95 kg m^{-3} for seawater of salinity $S = 35$ at 10°C and at one normal atmosphere). The propulsive force's application point $\mathbf{x}_0 = (-b/10, 0, 0)$, so that $\beta = (b + b/10)/b = 1.1$; the copepod's excess weight is chosen as $W_{excess} = 1.7438 \times 10^{-7}$ N (equivalent to assuming an excess density, defined as $\Delta\rho = \rho_c - \rho_w$, of 5.9 kg m^{-3}).

Using the above-described method, we have reconstructed an unsteady flow velocity vector field around the model copepod for the observed *E. rimana* adult female's unsteady swimming (figure 1*b*; 4.33–21.67 s in figure 2). From this time-varying flow-velocity vector field, we have calculated
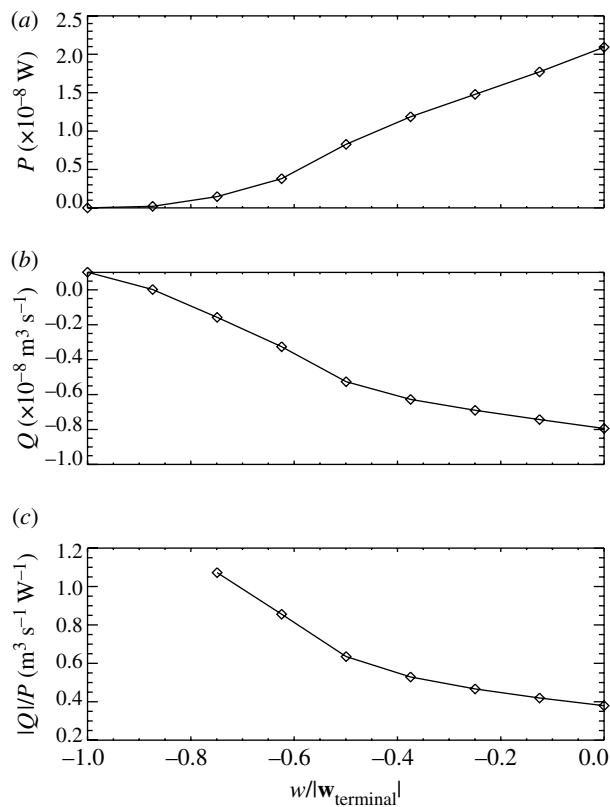
Figure 10. (*a*) Mechanical power, *P*, expended by a partially sinking model copepod in creating the flow field as a function of the partial-sinking speed (normalized by the terminal sinking velocity); (*b*) volumetric flux, *Q*, through the model copepod's capture area as a function of the normalized partial-sinking speed; (*c*) scanning efficiency, $|Q|/P$, as a function of the normalized partial-sinking speed. Note that fluxes of a negative sign (−) are downward (negative *z*-direction) fluxes.

trajectories of particles of many different initial positions. The results show that only those particles initially located within a tiny region ventral to the model copepod travel along a spiral-like unclosed curve similar to the observation. An example of such modelled algal trajectories is shown in figure 9*a*. The modelled two components (equations (2.6) and (2.7)) of the unsteady propulsive force are shown in figure 9*b*,*c*. It is found that the main flow direction and intensity is determined by the unsteady propulsive force's vertical component, the magnitude of which decreases slightly over time. On the other hand, the horizontal flow direction ventral to the spherical model copepod (whether towards the negative *x*-direction or the positive *x*-direction) is modulated strongly by the unsteady propulsive force's horizontal component (velocity vector plots are not shown). It seems that the observed algal trajectory over a long time period is a direct outcome of the dynamic coupling between the copepod's unsteady swimming and the unsteady flow field created by the copepod at its body scale. It is also shown that the contribution from inertia (body inertia + added mass term) is negligible when compared with the contribution from body drag and excess weight (figure 9*b*,*c*).

(iii) *Scanning efficiency within the partial sinking behaviour*
Using CFD, we have simulated the flow-velocity vector field around a model copepod performing the partial sinking behaviour with different sinking speeds. The size and morphology of the model copepod is similar to that of a typical *E. rimana* female. The excess weight of the model

copepod is set to be 1.7438×10^{-7} N, the same as that of the spherical model copepod in figure 9. The numerical simulation method is described in detail in the appendix, which can be accessed online as electronic supplementary material available at http://dx.doi.org/10.1098/rstb.2007.2081. For each simulated flow-velocity vector field, we have calculated the mechanical power, *P*, needed in creating the flow field around the model copepod (figure 10*a*), the volumetric flux, *Q*, through the capture area of the model copepod (figure 10*b*), and the scanning efficiency defined as $|Q|/P$ (figure 10*c*). It is shown that when the model copepod increases its partial sinking speed by exerting a smaller propulsive force to the water, less mechanical power is expended (figure 10*a*), and the volume of water the copepod scans in a given time interval also decreases (figure 10*b*). On the contrary, the scanning efficiency increases with increasing the partial sinking speed (figure 10*c*). In other words, when a copepod sinks faster and faster, starting at hovering and ending at free-sinking (i.e. through the entire range of partial sinking speeds), it will scan a greater volume of water for a given amount of mechanical energy expended, i.e. it has a higher mechanical energetic efficiency. This result may be applied to understand the observed unsteady swimming event of the *E. rimana* female as pictured in figures 1 and 2. In the very beginning, the copepod detects, by remote means, the location of an interesting algal particle. Upon detection, the copepod modulates its swimming behaviour to achieve greater energetic efficiency while still maintaining a tight control of the trajectory of the algal particle. Such a modulation process is energetically more efficient than exerting a constant propulsive force onto the water to create a constant feeding current of a wider entrainment range. A probable reason for this is that the flow modulation enables the copepod to avoid scanning a large amount of water parcels which are unlikely to contain valuable food particles.

(iv) *Kinematic influence of copepod-created flows on surrounding water parcels*
A parametric modelling study has been carried out to examine how the water flow created by a free-swimming copepod at its body scale moves, deforms, splits and stirs up the water/materials surrounding the copepod. The spherical model copepod is exactly the same as that described in figure 9 and swimming behaviour is taken as the only parameter that varies. Three swimming behaviours are considered: (i) hovering, (ii) partial sinking at half of the spherical model copepod's terminal sinking velocity, and (iii) the unsteady swimming behaviour as described in figure 1*b* and figure 2 (4.33–21.67 s). A cloud of fluid particles on the spherical model copepod's median plane at the ventral side is used to mark a water parcel which is initially disk-shaped and identical for all the three swimming behaviours considered. The cloud of fluid particles is then tracked numerically until the evolution of the water parcel under the influence of each of the three copepod-created flows is seen. It is shown that the water parcel is deformed, but still maintains an integrative shape when entrained into the feeding current created by the hovering copepod and stops deforming after passing by the copepod (figure 11). For the partial sinking behaviour, the water parcel is split into two portions: a large portion of the water parcel is entrained into the circulatory flow pattern created by the copepod and elongated and folded into a long, thin, spiral-like filament; a smaller portion of the water parcel is not entrained into the flow but elongates and later remains unaffected as the
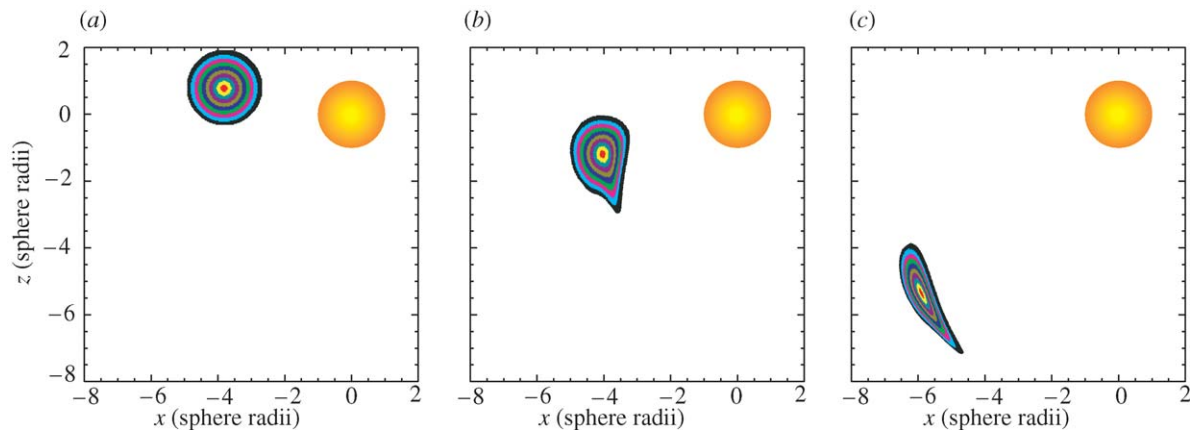
Figure 11. Kinematic influence, exerted by the flow field associated with a hovering spherical model copepod, on the motion of a water parcel initially located at the ventral side of the model copepod. (*a*) 0.0 s; (*b*) 0.6 s; (*c*) 2.4 s. See text for further explanation. An animation of this process can be viewed online (electronic supplementary material, animation 1).

copepod sinks further down (figure 12). For the unsteady swimming behaviour, irregular deformation, splitting, elongation and filamentation of the water parcel are imposed by the copepod-created unsteady flow (figure 13).

3. DISCUSSION

A full range of parametric studies based on a hydrodynamic model for copepod self-propelled swimming have provided an integrative picture of how basic flow modes of different flow-field patterns vary systematically and continuously with different basic steady translational swimming behaviours, i.e. free sinking, partial sinking, hovering, vertical swimming upward and horizontal swimming backward or forward. In fact, every copepod swimming behaviour results from the copepod applying a propulsive force of suitable magnitude and direction to the surrounding water to propel itself through the water in a certain way. By altering this propulsive force, a copepod is able to switch between different swimming behaviours and therefore is able to create surrounding flows of completely different flow-field patterns. From the viewpoint of a copepod, the propulsive force together with the body swimming motion creates a steady flow field, which can affect the surrounding water at a certain range and in a certain direction, depending on the steady swimming behaviour. As such, in theory, a copepod is able to transport any parcel of water, located at any distance and direction with respect to itself, to any desired place nearby itself (including its capture area). To facilitate such a rich variety of behavioural–fluid dynamical interaction and to create those small-scale fluid dynamical phenomena, a copepod must maintain a finite mass–density contrast against the surrounding water (Jiang & Strickler 2005). A neutrally buoyant copepod may be observed to swim actively in all directions, but in each swim, the associated surrounding flow resembles that created by a stresslet with its separation vector aligned with the swim direction (e.g. Visser 2001). A neutrally buoyant copepod would not be able to create the entire spectrum of flow-field patterns as revealed by the present study.

Furthermore, the propulsive force can vary temporally over long intervals, which is equivalent to a modulation of the basic flow modes. Such modulation leads to a time-varying swimming behaviour, or a sequence of swimming behaviours, and an unsteady flow field is created around the copepod. This point has been confirmed by the present modelling study reproducing the observed unsteady swimming event of an *E. rimana* female. The results suggest that the swimming trajectory of a copepod observed for tens of seconds with spatial extension over tens of body lengths is closely related to the unsteady flow field at the copepod's body scale. In other words, the swimming trajectory is a direct outcome of the body-scale flows and the dynamic coupling between the copepod's unsteady swimming and the unsteady flow field created by the copepod at its body scale. This is probably also true for many other aquatic micro-organisms.

Previous studies with tethered copepods have shown that individual capture events involve precise handling of algal particles at the copepod's appendage scale (e.g. Koehl & Strickler 1981; Paffenhöfer *et al.* 1982; Cowles & Strickler 1983). The study by Cowles & Strickler (1983) further shows that the copepod alternates between periods of rhythmic mouthpart movement (active swimming) and periods of no mouthpart movement (free sinking), a scenario similar to what we consider here as modulation of the basic flow modes. At its body scale, can a free-swimming copepod manipulate precisely the path of an entrained alga? The rerouting scenario described by Strickler (1985) shows that this can be done. Our modelling study reproducing the trajectory of an entrained alga (figure 9) shows that this can be done via modulation of the propulsive force (equivalent to modulation of the basic flow modes), and we further explain this in terms of the dynamic coupling between the copepod's unsteady swimming and the unsteady flow field created by the copepod at its body scale. This reveals a rather complex behavioural–fluid dynamical interaction among a copepod's unsteady free-swimming motion, unsteady flows around its body and the resulting trajectories of entrained algal particles.

Within its surrounding laminar water layers, a copepod modulates its self-created flow to manipulate precisely the trajectories of entrained algal particles and to single out good-quality algae and food items based
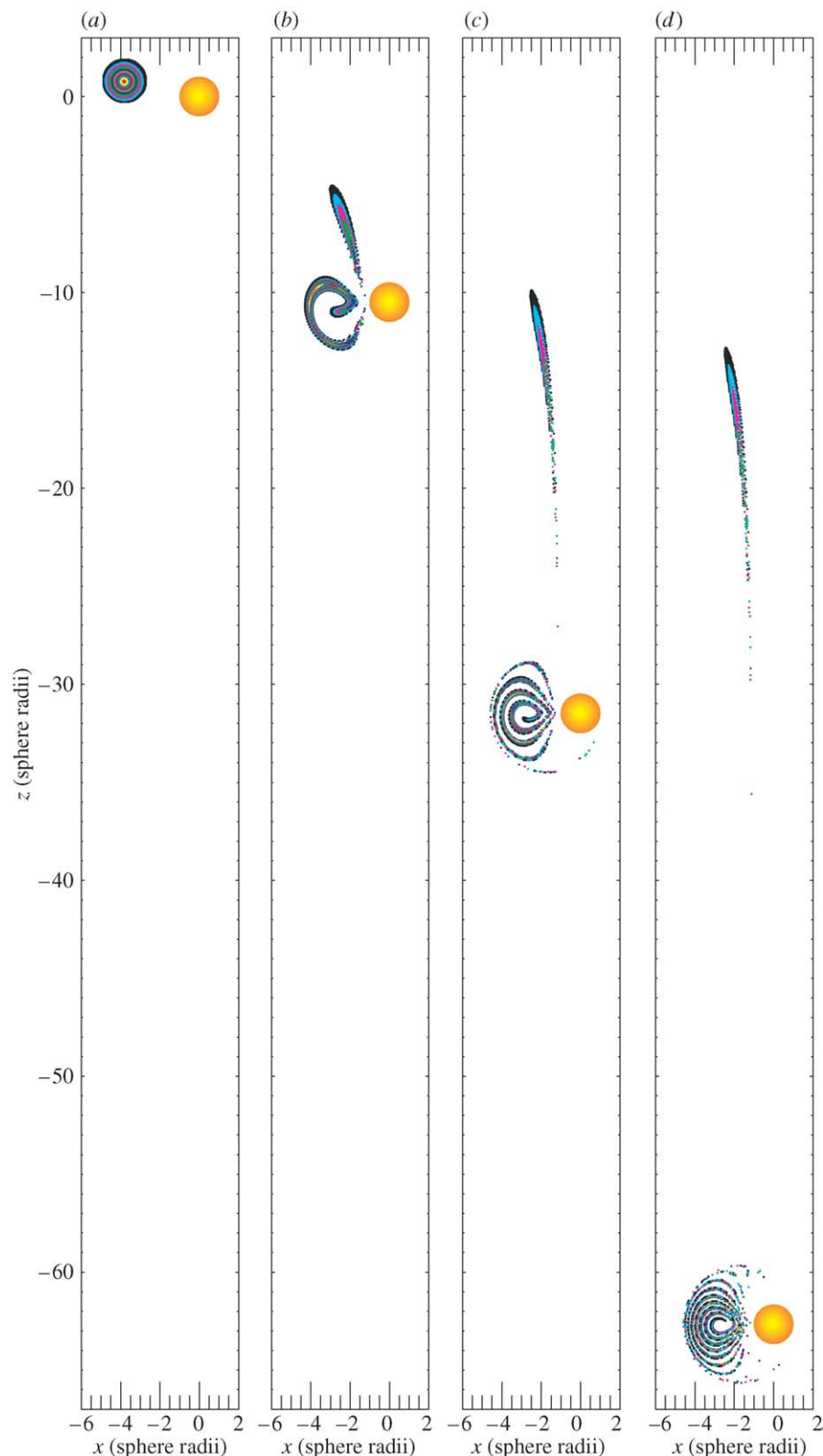
Figure 12. Kinematic influence, exerted by the flow field associated with a spherical model copepod sinking partially at half of its terminal sinking velocity, on the motion of a water parcel initially located at the ventral side of the model copepod. A stationary frame of reference is used. (*a*) 0.00 s; (*b*) 2.52 s; (*c*) 7.56 s; (*d*) 15.04 s. See text for further explanation. An animation of this process can be viewed online (electronic supplementary material, animation 2).

on advanced warning via chemoreception and/or mechanoreception. As supported by our CFD simulation results (figure 10*c*), the process involving modulation of the propulsive force may be energetically more efficient than exerting a constant propulsive force onto the water to create a constant feeding current.

A constant feeding current leads to a wider entrainment range (figure 11). By contrast, the flow field surrounding a partially sinking copepod (figure 12) and that surrounding an unsteadily swimming copepod (figure 13) split a water parcel into two portions. If the entrained portion contains food and the
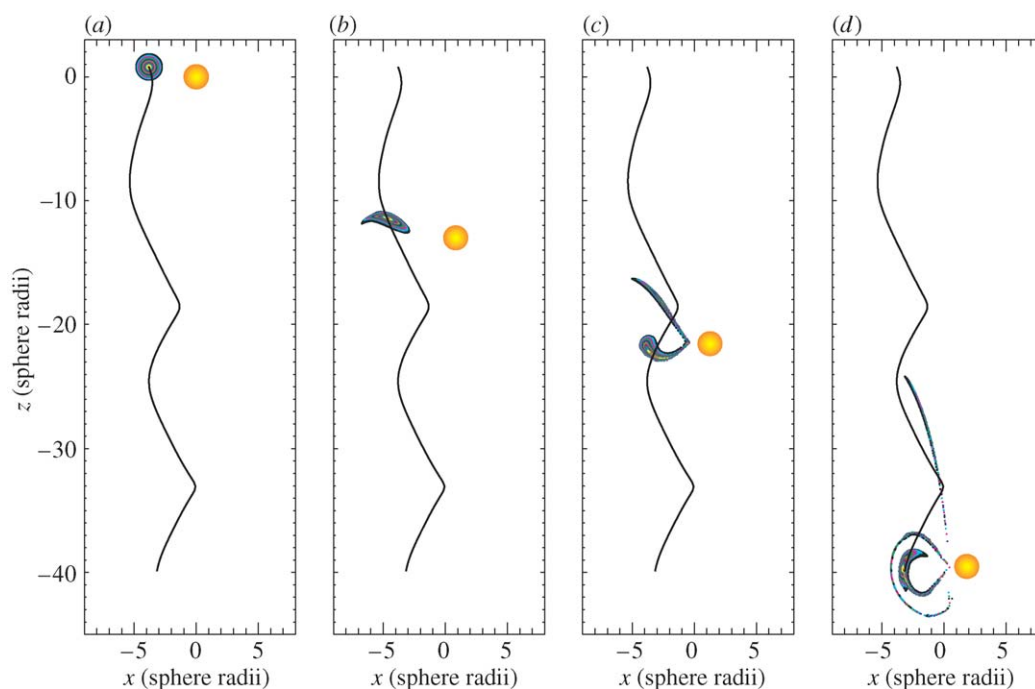
Figure 13. Kinematic influence, exerted by the flow field associated with a spherical model copepod swimming at a time-varying velocity $\mathbf{U}(t)$ of the same two components as those shown in figure 2 (4.33–21.67 s), on the motion of a water parcel initially located at the ventral side of the model copepod. The curved solid line is the trajectory of the same particle as shown in figure 9 and here a stationary frame of reference is used. (*a*) 4.33333 s; (*b*) 11.2933 s; (*c*) 14.7733 s; (*d*) 21.6533 s. See text for further explanation. An animation of this process can be viewed online (electronic supplementary material, animation 3).

unentrained portion contains no food, energetic efficiency is certainly achieved. There is no need to scan the extra large amount of water within which there are no valuable algae or food particles. This is a strategy to deal with one-by-one encounters with algal particles and food items, a situation due to discrete distribution of phytoplankton and food items at the body scale of a copepod. A probable additional benefit for a partially sinking copepod is that the circulatory flow pattern keeps the entrained food items within the feeding current for a longer time allowing subsequent ingestion by a copepod which has food in its mouthparts and needs time to handle the food (the food handling process does occur as described by Strickler 1984).

Our modelling study shows that a copepod-created flow may deform and stir up the surrounding water and materials, depending strongly on the swimming behaviour. For the partial sinking behaviour, strong stirring-up leads to sharp gradients (figure 12) which may benefit the transport of materials from and to the copepod with the aid of diffusion. For the unsteady swimming behaviour considered, chaotic mixing even occurs in some tiny regions surrounding the spherical model copepod (figure 13). Heuristically, and in the simplest picture, chaotic mixing happens when streamline portraits viewed at different times show streamline crossing (Ottino & Wiggins 2004). Such a scenario probably happens for the unsteady flow created by a copepod swimming unsteadily over a long time period and for the overlapped flows created by a swarm of randomly swimming copepods.

In terms of methodology, we apply a relatively simple hydrodynamic model which has an analytical solution to a rather complex problem of unsteadiness in copepod-created flows. To achieve this, simplifications, such as assuming a spherical body shape and neglecting the inertial terms in the Navier–Stokes equation, are made. For simplicity, we choose not to use the unsteady Stokes equation the solution of which needs Fourier-transform. For the dynamic equation of the spherical model copepod, the body inertia and the added mass term are included, though their contribution is shown to be negligible. Koehl *et al.* (2003) has shown that the Bassett-history term (the memory-integral term) is important for the gravitational settling of particles in the size range of 0.1–10 mm (e.g. many larger phytoplankton cells and chain-formers). We are not able to include the memory-integral term into our calculations. One of the reasons for this is that the form of the memory-integral term itself is unknown for the present situation where the flow around the spherical model copepod is strongly affected by the flow induced by the propulsive force. However, our simple model has provided a satisfactory solution, as demonstrated by a comparison between the modelling result and the observational result. (Some discrepancy does exist at the final stage when the copepod approaches the bottom of the aquarium.) More complex methods involving numerical simulations may be used to consider all the terms neglected and realistic morphology. However, the conclusion would most likely be the same as that obtained in this study.

Almost no observational data can be found in the literature about the unsteadiness and modulation of copepod-created flows. Our suggestions for observational studies along this line are: on one hand, the observation should provide the three-dimensional trajectory and body orientations of a copepod swimming freely over a long time period (e.g. tens of seconds with a length-scale of tens of body lengths); on the

other hand, the observation should be able to provide simultaneously a time-series of the unsteady flow field at the copepod's body scale with detailed enough information about the paths of entrained algae and individual capturing events.

Another question is how a copepod adjusts its appendage movements for accomplishing modulation of the propulsive force as well as power output. To answer this question, detailed observations should be made at the appendage scale, which measure the variations in beating frequencies, attack angles and amplitudes of beating movements. It would be even better to carry out these measurements simultaneously with the previously outlined observations for understanding the processes at the body scale and at the scale of tens of body lengths.

Finally, we provide speculation on how a free-swimming copepod may interact with the smallest eddies of small-scale oceanic turbulence. The modulation of the basic flow modes occurs at a length-scale of up to a few body lengths and a time-scale of up to tens of seconds. At these spatial and temporal scales, some small-scale flow structures of the turbulence still form, including vortices, shears, stagnation points and jet streams. These organized energy-containing small-scale flow structures overlap with the biologically created flow fields, leading to more complex flow patterns. The challenge for a copepod may be how to exploit the mechanical energy by staying in certain flow structures, by avoiding certain flow structures and/or adopting certain unsteady translational/rotational swimming behaviours with suitable body orientations relative to (outside or inside) the flow structures. To capture as many algae/food items as possible, while expending as little energy as possible may be a criterion. A numerical simulation study has been carried out to test the hypothesis that a planktonic organism could reduce the cost of hovering by making use of the local flow structures of turbulence (Yamazaki *et al.* 2004). More modelling, numerical and observational studies are needed along this line.

REFERENCES

Bundy, M. H. & Paffenhöfer, G.-A. 1996 Analysis of flow fields associated with freely swimming calanoid copepods. *Mar. Ecol. Prog. Ser.* **133**, 99–113.

Bundy, M. H. & Vanderploeg, H. A. 2002 Detection and capture of inert particles by calanoid copepods: the role of the feeding current. *J. Plankton Res.* **24**, 215–223. (doi:10.1093/plankt/24.3.215)

Cowles, T. J. & Strickler, J. R. 1983 Characterization of feeding activity patterns in the planktonic copepod *Centropages typicus* Kroyer under various food conditions. *Limnol. Oceanogr.* **28**, 105–115.

Jiang, H. 2004 Numerical simulation of the flow field at the scale size of an individual copepod. In *Handbook of scaling methods in aquatic ecology: measurement, analysis, simulation* (eds L. J. Seuront & P.G Strutton), pp. 479–491. Boca Raton, FL: CRC Press.

Jiang, H. & Strickler, J. R. 2005 Mass density contrast in relation to the feeding currents in calanoid copepods. *J. Plankton Res.* **27**, 1003–1012. (doi:10.1093/plankt/fbi087)

Jiang, H., Osborn, T. R. & Meneveau, C. 2002*a* The flow field around a freely swimming copepod in steady motion. Part I. Theoretical analysis. *J. Plankton Res.* **24**, 167–189. (doi:10.1093/plankt/24.3.167)

Jiang, H., Meneveau, C. & Osborn, T. R. 2002*b* The flow field around a freely swimming copepod in steady motion. Part II. Numerical simulation. *J. Plankton Res.* **24**, 191–213. (doi:10.1093/plankt/24.3.191)

Koehl, M. A. R. & Strickler, J. R. 1981 Copepod feeding currents: food capture at low Reynolds number. *Limnol. Oceanogr.* **26**, 1062–1073.

Koehl, M. A. R., Jumars, P. A. & Karp-Boss, L. 2003 Algal biophysics. In *Out of the past* (ed. T. A. Norton), pp. 115–130. Belfast, Northern Ireland: British Phycological Association.

Malkiel, E., Shen, J., Katz, J. & Strickler, J. R. 2003 The three-dimensional flow field generated by a feeding calanoid copepod measured using digital holography. *J. Exp. Biol.* **206**, 3657–3666. (doi:10.1242/jeb.00586)

Ottino, J. M. & Wiggins, S. 2004 Designing optimal micromixers. *Science* **305**, 485–486. (doi:10.1126/science.1099343)

Paffenhöfer, G.-A., Strickler, J. R. & Alcaraz, M. 1982 Suspension-feeding by herbivorous calanoid copepods: a cinematographic study. *Mar. Biol.* **67**, 193–199. (doi:10.1007/BF00401285)

Strickler, J. R. 1982 Calanoid copepods, feeding currents, and the role of gravity. *Science* **218**, 158–160. (doi:10.1126/science.218.4568.158)

Strickler, J. R. 1984 Sticky water: a selective force in copepod evolution. In *Trophic interactions within aquatic ecosystems* (eds D. G. Meyers & J. R. Strickler), pp. 187–239. Washington, DC: American Association for the Advancement of Science.

Strickler, J. R. 1985 Feeding currents in calanoid copepods: two new hypotheses. In *Physiological adaptations of marine animals* (ed. M. S. Laverack), pp. 459–485. Cambridge, UK: The Company of Biologists.

Tiselius, P. & Jonsson, P. R. 1990 Foraging behaviour of six calanoid copepods: observations and hydrodynamic analysis. *Mar. Ecol. Prog. Ser.* **66**, 23–33.

Visser, A. W. 2001 Hydromechanical signals in the plankton. *Mar. Ecol. Prog. Ser.* **222**, 1–24.

Yamazaki, H., Squires, K. D. & Strickler, J. R. 2004 Can turbulence reduce the energy costs of hovering for planktonic organisms? In *Handbook of scaling methods in aquatic ecology: measurement, analysis, simulation* (eds L. J. Seuront & P. G. Strutton), pp. 493–506. Boca Raton, FL: CRC Press.

Yen, J., Sanderson, B., Strickler, J. R. & Okubo, A. 1991 Feeding currents and energy dissipation by *Euchaeta rimana*, a subtropical pelagic copepod. *Limnol. Oceanogr.* **36**, 362–369.